



University of
New Haven

University of New Haven

Digital Commons @ New Haven

Chemistry and Chemical Engineering Faculty
Publications

Chemistry and Chemical Engineering

10-3-2018

Au@h-Al₂O₃ Analogic Yolk–Shell Nanocatalyst for Highly Selective Synthesis of Biomass-Derived D-xylonic Acid via Regulation of Structure Effects

Jiliang Ma
South China University of Technology

Zewei Liu
South China University of Technology

Junlong Song
Nanjing Forestry University

Linxin Zhong
South China University of Technology

Dequan Xiao
University of New Haven, DXiao@NewHaven.edu

See next page for additional authors

Follow this and additional works at: <https://digitalcommons.newhaven.edu/chemicalengineering-facpubs>



Part of the [Chemical Engineering Commons](#), and the [Chemistry Commons](#)

Publisher Citation

Ma, Jiliang, Zewei Liu, Junlong Song, Linxin Zhong, Dequan Xiao, Hongxia Xi, Xuehui Li, Run-Cang Sun, and Xinwen Peng (2018). "Au@ h-Al₂O₃ analogic yolk-shell nanocatalyst for highly selectively synthesis of biomass-derived D-xylonic acid via regulation of structure effect." *Green Chemistry* 20:5188-5195.

Comments

This is the authors' accepted manuscript of the article published in *Green Chemistry*. The published version can be found at <http://dx.doi.org/10.1039/C8GC02618A>

Authors

Jiliang Ma, Zewei Liu, Junlong Song, Linxin Zhong, Dequan Xiao, Hongxia Xi, Xuehui Li, Runcang Sun, and Xinwen Peng

1 **Au@h-Al₂O₃ analogic yolk-shell nanocatalyst for highly**
2 **selectively synthesis of biomass-derived D-xylonic acid via**
3 **regulation of structure effect**

4 Jiliang Ma,^a Zewei Liu,^{a,c} Junlong Song,^b Linxin Zhong,^{*a} Dequan Xiao,^d
5 Hongxia Xi,^c Xuehui Li,^c Runcang Sun ^{*c} and Xinwen Peng ^{*a}

6 ^a State Key Laboratory of Pulp and Paper Engineering, South China
7 University of Technology, Guangzhou, China. 510641.

8 ^b Jiangsu Co-Innovation Center for Efficient Processing and Utilization of
9 Forest Resources, Nanjing Forestry University, Nanjing, China.

10 ^c School of Chemistry and Chemical Engineering, South China
11 University of Technology, Guangzhou, China.

12 ^d Center for Integrative Materials Discovery, Department of
13 Chemistry and Chemical Engineering, University of New Haven, West
14 Haven, CT 06516.

15 ^e Institute of Biomass Chemistry and Utilization, Beijing Forestry
16 University, Beijing, China.

17

18

19

20

21 *Corresponding authors' E-mail: fexwpeng@scut.edu.cn (Xinwen Peng),
22 lxzhong0611@scut.edu.cn (Linxin Zhong) and rcsun3@bjfu.edu.cn
23 (Runcang Sun), Tel.: +86-020-87111860; Fax: +86-020-87111860.

24 **Abstract**

25 Selective oxidation of biomass-based monosaccharides into value-added
26 sugar acids is highly desired, yet limited success of producing D-xylonic
27 acid has been achieved. Here, we report an efficient catalyst system, Au
28 nanoparticles anchoring on the inner wall of hollow Al₂O₃ nanospheres
29 (Au@h-Al₂O₃), which could catalyze the selective oxidation of D-xylose
30 into D-xylonic acid under base-free conditions. The mesoporous Al₂O₃
31 shell as adsorption sites first adsorbed D-xylose, the interface of Au
32 nanoparticles and Al₂O₃ as active sites spontaneously dissociated O₂, and
33 the exposed Au nanoparticles surface as catalytic sites drove the
34 transformation. With this catalyst system, the valuable D-xylonic acid was
35 produced with excellent yields in the aerobic oxidation of D-xylose.
36 Extensive works showed that the Au@h-Al₂O₃ is an efficient catalyst
37 with highly stability and recycling.

38

39

40

41

42

43

44

45

46 **Key words:** D-xylose · D-xylonic acid · Au@h-Al₂O₃ · structural effect
47 regulation system · selective oxidation

48 **Introduction**

49 Use of biomass-derived feedstocks provides an environmentally friendly
50 and sustainable route for the production of chemicals. Organic acid is a
51 versatile, renewable chemical with a wide industrial application profile
52 both as a solvent and as a building block.^{1,2} It is also widely used in food,
53 pharmaceutical, cosmetic, detergent, polymer, and textile.^{3,4}
54 Transformation of biomass into value-added organic acids is highly
55 desired, but is still very limited owing to the lack of efficient catalytic
56 system and method. Recently, monosaccharide oxidation (especially
57 selective oxidation), as a crucial element of organic acid production,
58 offers an attractive option on the conversion of biomass resources into
59 chemicals and sugar acids.

60 D -Xylose, one of the main sugar units in hemicelluloses, is the
61 second most abundant sugar in nature.⁵ Many efforts have been made on
62 utilizing of D -xylose by fermenting⁶ or other processes to obtain fuels and
63 chemicals.⁷⁻¹⁰ Among these products, D -xylonic acid is one of the top 30
64 high-value chemicals identified by the US Department of Energy. It is a
65 key compound for the preparation of 1,2,4-butanetriol or energetic
66 materials 1,2,4-butanetriol trinitrate.¹¹ Currently, as a concrete additive,
67 D -xylonic acid can effectively improve concrete dispersion.¹² Furthermore,
68 D -xylonic acid can be used as an efficient biocatalyst for organic
69 transformations.¹³ Other applications of D -xylonic acid have been
70 reported in food, pharmaceutical, and agriculture.^{14,15} Therefore,
71 innumerable scientists have devoted to themselves to the synthesis of D -
72 xylonic acid research. Among all the literatures, microbial production of
73 D -xylonic acid plays a significant role in the synthesis of D -xylonic acid.
74 As early as 1946, Lockwood and Nelson reported that the production of
75 D -xylonic acid could occur in the *Pseudomonas*.¹⁶ Later, a lot of studies

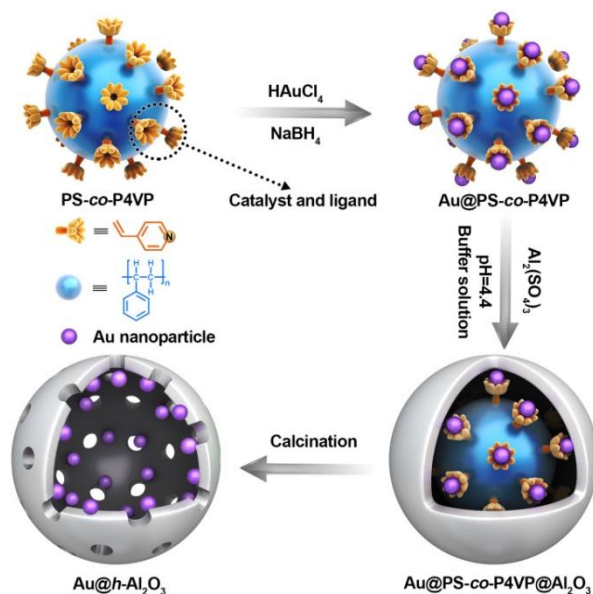
76 have found that D-xylonic acid could be produced in the oxidative
77 metabolism of D-xylose by some archaea and bacteria.^{9, 17-20} But until now,
78 commercial production of D-xylonic acid has not been developed,
79 reflecting the current limited market for D-xylonic acid. The reason lies in
80 two facts: the one is that many others oxidizing enzymes are produced by
81 bacteria strains which directly contribute to the conversion of other sugars
82 present in lignocellulosic hydrolysates, the other is that the engineered
83 yeast strains have low D-xylonic acid accumulation rate and yield.⁹
84 Besides, industrial scale production of D-xylonic acid needs the high cost
85 of peptone and/or yeast extract media as nitrogen sources, which decide
86 that the production methods are impractical. Furthermore, although the
87 application of chemical synthesis in industrial production is widespread,
88 few studies have been reported for the synthesis of D-xylonic acid by
89 chemical synthesis.

90 Au-based catalysts are found to be superior to Pt, Pd and Pt/Pd
91 bimetallic catalysts for the oxidation of glucose to gluconic acid,²¹ as Au
92 nanoparticles (NPs) have low sensitivity to oxygen poisoning and high
93 activity in a wide range of pH values. However, the free Au NPs with
94 high surface energy are easy to agglomerate, which affect its activity. To
95 avoid this drawback, functional supports with a strong interaction with
96 Au,²²⁻²⁶ pores²⁷⁻³⁰ and core/yolk-shell architecture³¹⁻³³ are developed to
97 improve the stability of Au NPs. The core/yolk-shell architecture featured
98 the advantages of high permeability, low density, large surface area,
99 multifunctionality, and high loading capacity,^{31, 34-38} Furthermore,
100 modification of the core/yolk-shell structure to give a nanocatalyst with
101 metal NPs embedded on its inner wall can not only improve the stability
102 of metal NPs, but also generate a synergistic effect on the interface
103 between the metal NPs and the shell.^{39, 40}

104 Herein, we report a new catalyst of Au NPs anchoring on the inner
105 wall of mesoporous hollow Al₂O₃ nanospheres, prepared via the
106 technique of core/yolk-shell architecture. The Au@*h*-Al₂O₃ catalyst can
107 selectively oxidize D-xylose to D-xylonic acid. The correlation between
108 the unique structure and catalytic activity of Au@*h*-Al₂O₃ was revealed
109 through comparative experiments. The adsorption sites were investigated
110 by a technique called quartz crystal microbalance with dissipation
111 monitoring (QCM-D) and DFT calculations. The active sites for the
112 spontaneous dissociation of O₂ were studied by DFT calculations. The
113 catalytic sites of Au@*h*-Al₂O₃ were verified by the comparison
114 experiment of sulfhydryl coated surface of Au NPs.

115 **Results and discussion**

116 The synthetic scheme of the Au@*h*-Al₂O₃ is shown in Fig. 1. A soap-free
117 emulsion polymerization method was adopted to prepare a core/shell
118 structure of PS-*co*-P4VP,⁴¹ which was then used as scaffold for the
119 immobilization of Au NPs. The dispersed Au NPs were then anchored
120 onto the PS-*co*-P4VP core/shell microspheres by coordination of Au³⁺
121 (from HAuCl₄) with the P4VP shell first and then by reduction with
122 NaBH₄.⁴¹ Afterwards, uniform layers were gradually growing onto the
123 surface of Au@PS-*co*-P4VP by controlling the precipitation process in a
124 buffer solution of formic acid-ammonium formate.⁴² Finally, the resultant
125 NPs were calcined to remove PS-*co*-P4VP and allow the Au NPs to be
126 distributed on the inner wall of the hollow Al₂O₃ sphere. In this process,
127 PS-*co*-P4VP microspheres played a dual role, a scaffold for
128 immobilization of dispersed Au NPs⁴¹ and a template for the synthesis of
129 Al₂O₃ coating.



130

131

Fig. 1 Schematic illustration of the synthetic route of Au@h-Al₂O₃.

132

133

134

135

136

137

138

139

140

141

142

143

144

145

146

147

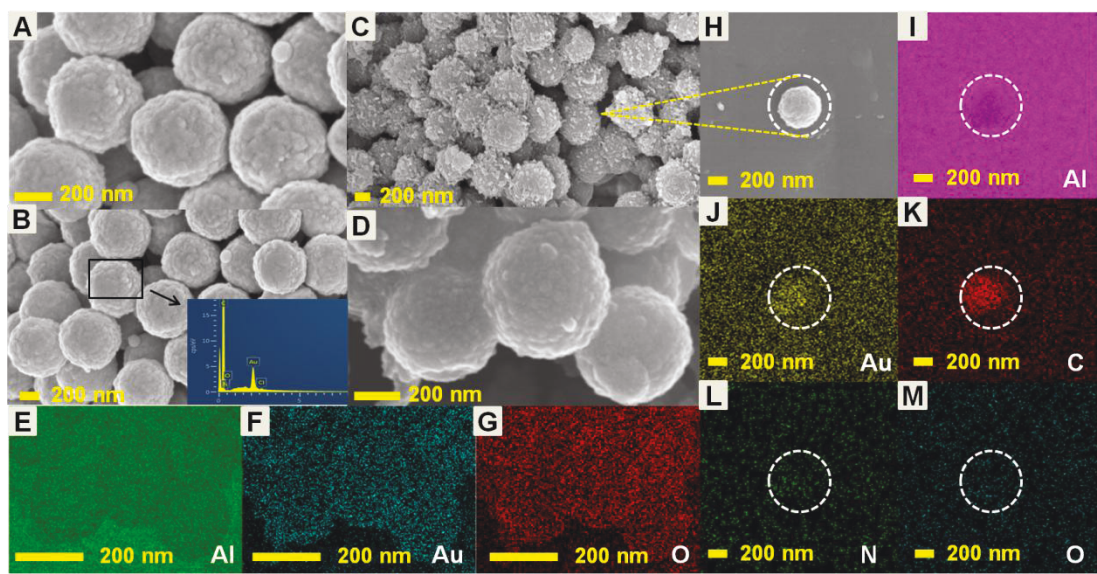
148

The morphology and chemical composition of the intermediate and Au@h-Al₂O₃ were first characterized by scanning electron microscope (SEM). As shown in Fig. 2A, the pure PS-co-P4VP microspheres with an average size of about 490 nm were observed. As compared with the PS-co-P4VP microspheres, Au@PS-co-P4VP microspheres showed no significant difference on morphology and size (Fig. 2B). The elements of Au@PS-co-P4VP were mainly Au, C, O and N (the inset of Fig. 2B), indicating that Au NPs were successfully deposited on the surface of PS-co-P4VP. After the precipitation of Al₂O₃ on the surface of Au@PS-co-P4VP microspheres (using Al₂(SO₄)₃ as the precursor of Al₂O₃), a thin shell was coated to produce Au@PS-co-P4VP@Al₂O₃ microspheres, which was confirmed by a slight increase in the size from 490 to 510 nm (Fig. 2C, 2H). The elemental mapping of O, Al, Au, C and N (Fig. 2I-2M) further evidenced the successful preparation of Au@PS-co-P4VP@Al₂O₃ microspheres. After Au@PS-co-P4VP@Al₂O₃ NPs were calcined at 550 °C, the polymeric template was removed, and Au NPs were left on the inner wall of hollow Al₂O₃ sphere, producing Au@h-Al₂O₃ (Fig. 2D and

149 Supporting Information Fig. S1). Only Al, Au and O were observed in the
150 EDX area scanning of Au@*h*-Al₂O₃, which indicates that the cavity
151 structure was achieved after the calcination (Fig. 2E-G).

152 The transmission electron microscopy (TEM) image of pure PS-*co*-
153 P4VP microspheres in Fig. S2A is consistent with the SEM results. In the
154 TEM images of Fig. S2B, the Au@PS-*co*-P4VP@Al₂O₃ microspheres
155 with a diameter of ~510 nm. The inter bright spots represent the PS-*co*-
156 P4VP core; the dark spots indicate the Au NPs, while the peripheral dark
157 circle corresponds to Al₂O₃ shell. After PS-*co*-P4VP core was removed,
158 the shell (of 10 nm in thickness) and the cavity were clearly observed by
159 TEM and STEM (Fig. 3A and 3B); and Au NPs with a diameter of ~1.87
160 nm were observed on the inner wall of Al₂O₃ microspheres (the inset in
161 Fig. 3B). Besides the diameter of Au NPs slightly increased from 1.87 to
162 2.20 nm (Supporting Information Fig. S3C), and no significant difference
163 in size was observed for Au@*h*-Al₂O₃ after being used for 10 times
164 (Supporting Information Fig. S3A, S3B and S4), indicating the high
165 stability of Au@*h*-Al₂O₃. The Au element analyzed with XPS is shown in
166 Fig. 3D. The signal of Au 4f can be resolved into two peaks. The binding
167 energies of Au 4f_{5/2} and Au 4f_{7/2} locating at 87.7 and 83.9 eV indicate Au⁰,
168 while the 89.6 and 86.3 eV demonstrate Au₂O₃, respectively.⁴³ There was
169 no significant difference in Au valence for Au@*h*-Al₂O₃ before and after
170 catalysis for *D*-xylose oxidation. For the freshly prepared Au@*h*-Al₂O₃,
171 the peaks locating at 83.9 and 87.5 eV reveal only the valence of Au
172 species. After being used for the synthesis of *D*-xylonic acid, the peaks
173 shift slightly to the lower binding energies at 83.5 and 87.3 eV
174 (Supporting Information Fig. S5), respectively, indicating that the valence
175 of Au species did not change much during the catalytic oxidation process.
176 In addition, the difference in O 1s and Al 2p spectra for Au@*h*-Al₂O₃ was

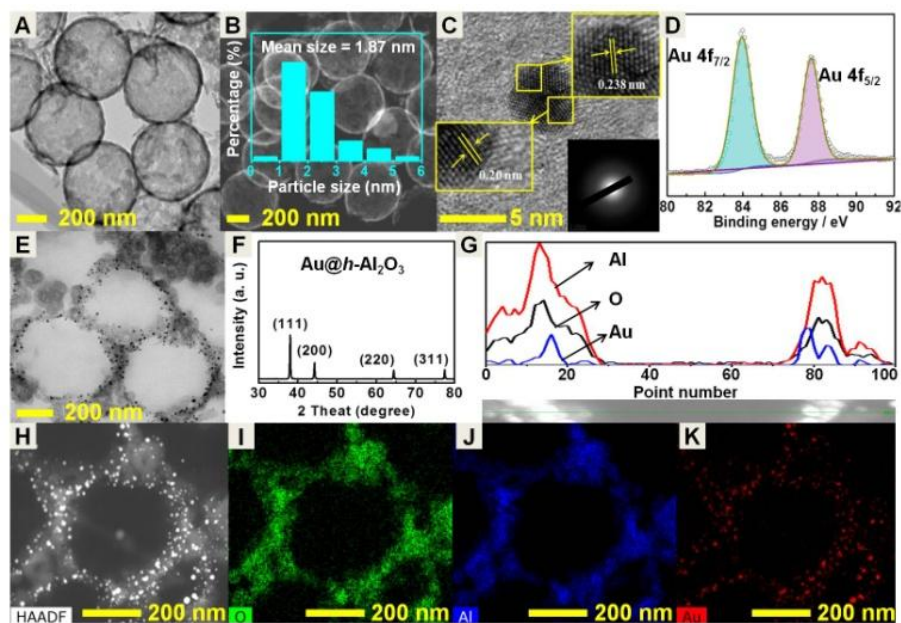
177 not significant before and after being used for D -xylose oxidation
178 (Supporting Information Fig. S6). The Au contents determined by ICP-
179 MS were 2.80 wt% and 2.49 wt% for Au@ h -Al₂O₃ before use and after
180 10 catalytic cycles, respectively, indicating that Au@ h -Al₂O₃ has
181 excellent stability (Supporting Information Table S1). Fig. S7A shows the
182 HAADF-STEM spectrum of Au@ h -Al₂O₃. The white spots indicate the
183 Au NPs and the peripheral white circle corresponds to the Al₂O₃ shell.
184 The elemental mapping of O, Al and Au in Au@ h -Al₂O₃ are shown in
185 Fig. S7B-D, demonstrating the actual distributions of O, Al, and Au
186 elements in the catalyst. Fig. 3C shows the HRTEM image of Au@ h -
187 Al₂O₃. There were mainly two types of lattice fringes with interplanar
188 spacing of 2.32 and 2.0 Å, corresponding to (111) and (200) crystal
189 planes of Au NPs, respectively. The inset in Fig. 3C shows the diffraction
190 pattern of Au NPs. To illustrate the position of Au NPs in Au@ h -Al₂O₃, a
191 STEM spectrum of Au NP is given in Fig. S8A; then a line scan of the
192 Au NP is shown in Fig. S8B, which gives a preliminary explanation of
193 the position of Au NPs in Au@ h -Al₂O₃. Fig. 3F shows the XRD pattern
194 of Au@ h -Al₂O₃ catalyst. Au@ h -Al₂O₃ displays a good crystallinity and
195 the diffraction peaks at $2\theta = 38.27^\circ$, 44.6° , 64.68° and 77.55° were
196 assigned to (111), (200), (220) and (311) reflections of the gold lattice,
197 well agreeing with the results from Fig. 3C. The 10th reused Au@ h -Al₂O₃,
198 Au/Al₂O₃ and other Au catalysts (Supporting Information Fig. S4F and
199 S9a-d) also showed the similar diffraction peaks.



200

201 **Fig. 2** SEM of PS-*co*-P4VP (A), Au@PS-*co*-P4VP (B) (the inset is the EDX of
 202 Au@PS-*co*-P4VP), Au@PS-*co*-P4VP@Al₂O₃ (C, H), Au@*h*-Al₂O₃ (D) and element
 203 mapping images of Au@*h*-Al₂O₃: Al element (E), Au element (F), and O element (G),
 204 the element mapping images of Au@PS-*co*-P4VP@Al₂O₃: Al element (I), Au
 205 element (J), C element (K), N element (L) and O element (M).

206 To further determine the distribution patterns of Al, O and Au in
 207 Au@*h*-Al₂O₃, Au@*h*-Al₂O₃ with 10 times HAuCl₄ addition was prepared
 208 and the obtained products were named Au@*h*-Al₂O₃-10. Besides an
 209 obvious increase in diameters of Au NPs (the inset in Supporting
 210 Information Fig. S10B), no significant difference was observed between
 211 Au@*h*-Al₂O₃-10 and Au@*h*-Al₂O₃ (Supporting Information Fig. S10A-E).
 212 The elemental mapping of Au@*h*-Al₂O₃-10 in Fig. S10F-H gave a clear
 213 distribution of O, Al and Au. The TEM and STEM of the cross section
 214 diagram of Au@*h*-Al₂O₃-10 visually showed the distribution of Au NPs
 215 (Fig. 3E, 3H and Supporting Information Fig. S11). The line scan
 216 spectrum and elemental mapping of the cross section diagram of Au@*h*-
 217 Al₂O₃-10 further presented the actual distributions of O, Al, and Au
 218 elements (Fig. 3G and 3I-3K). All the results demonstrated that Au NPs
 219 are well distributed on the inner wall of the Al₂O₃ hollow sphere.



220

221 **Fig. 3** TEM and STEM of Au@*h*-Al₂O₃ (A, B). The inset B is the size distributions of
 222 Au NPs from 300 particles. (C) High-resolution TEM image of Au@*h*-Al₂O₃ (the
 223 inset is the diffraction patterns of Au NPs). (D) Au 4f spectra for Au@*h*-Al₂O₃. (E)
 224 TEM of the cross section diagram of Au@*h*-Al₂O₃-10. (F) The XRD pattern of
 225 Au@*h*-Al₂O₃. (G) The line scan of cross section diagram of Au@*h*-Al₂O₃-10. (H)
 226 STEM-HAADF image of the cross section diagram of Au@*h*-Al₂O₃-10 and element
 227 mapping images: (I) O element, (J) Al element, and (K) Au element.

228 The N₂ sorption isotherms of Au/Al₂O₃, Au@PS-*co*-P4VP@Al₂O₃
 229 and Au@*h*-Al₂O₃ exhibit type IV isotherm patterns (Supporting
 230 Information Fig. S12), suggesting the presence of mesopores in these
 231 materials. Compared to Au/Al₂O₃ and Au@PS-*co*-P4VP@Al₂O₃, Au@*h*-
 232 Al₂O₃ showed more uniform and well-developed mesopores with a
 233 diameter of 2.19 nm, favoring the diffusion of reactants and products in
 234 and out of the catalyst. The BET results showed that the surface area of
 235 Au@*h*-Al₂O₃ increases from 10.09 to 100.45 m²/g after removing PS-*co*-
 236 P4VP, indicating a higher contact area between D-xylose and Au@*h*-
 237 Al₂O₃. Fig. S13 shows no significant difference in the thermal weight loss
 238 between Au@*h*-Al₂O₃ and Au/Al₂O₃, demonstrating that the catalysts
 239 have a good thermostability. Although weight loss occurs to Au@PS-*co*-

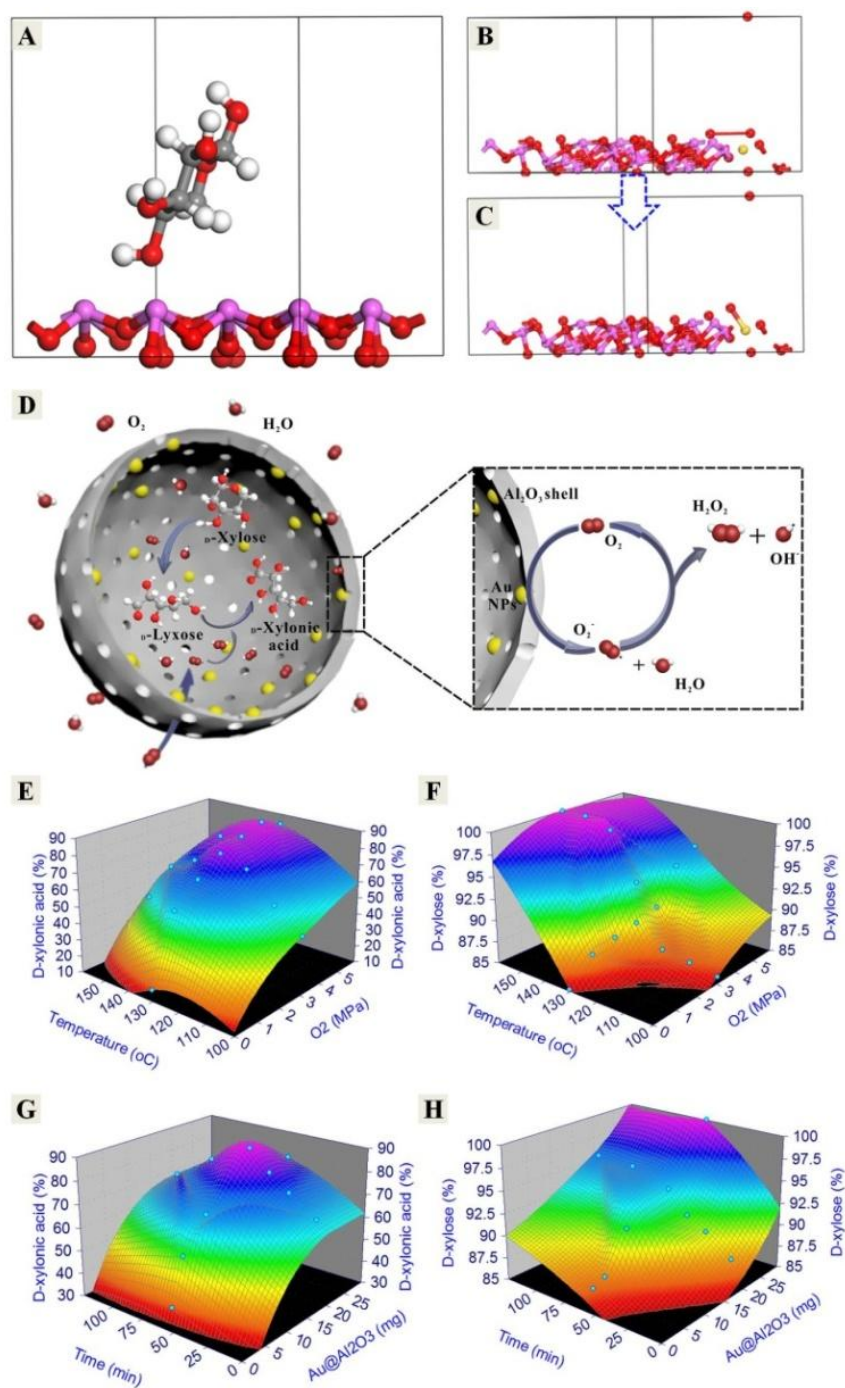
240 P4VP@Al₂O₃ when the temperature was higher than 350 °C, it has no
241 impact on the aerobic oxidation of D-xylose because the reaction was
242 carried out in the temperature range of 100-160 °C.

243 Prior to comprehensively investigate the catalytic activity of Au@h-
244 Al₂O₃ on the aerobic oxidation of D-xylose to D-xylonic acid, the affinities
245 of D-xylose to various surfaces (Al₂O₃, silica, and gold) were compared
246 by a technique of quartz crystal microbalance with dissipation monitoring
247 (QCM-D). Fig. S14 shows that the frequency change of Al₂O₃ surface is -
248 7.3 Hz after water rinsing, which is equivalent to 129.2 mg/m², higher
249 than those of silica (-1.4 Hz and 24.8 mg/m²) and gold (-4.9 Hz and 86.7
250 mg/m²) surfaces. The results suggest that Al₂O₃ has a much stronger
251 affinity to D-xylose than silica and gold.

252 The adsorption energy of D-xylose on Al₂O₃ was calculated by DFT
253 methods using DMOL3 module from Materials Studio 2017.⁴⁴ A model
254 of the dehydrated Al₂O₃ (110) surface (Fig. 4A), the same as that used by
255 Falamaki and co-workers,⁴⁵ was chosen to investigate the interactions
256 between D-xylose and the Al₂O₃ crystal. The adsorption energy of D-
257 xylose on Al₂O₃ (110) was -70 kJ/mol. In addition, the dissociation
258 energy O₂ on the interface of Au NPs and Al₂O₃ shell was also calculated
259 by DFT as -245.68 kJ/mol (Fig. 4B and 4C), suggesting that the O₂
260 molecule can be dissociated spontaneously on the interface of Au NPs
261 and Al₂O₃ shell. The generated negative oxygen ion is expected to react
262 with water to produce oxidizing substances. These results indicate that it
263 is feasible to synthesize D-xylonic acid from D-xylose catalyzed by
264 Au@h-Al₂O₃.

265 For the aerobic oxidation of D-xylose to D-xylonic acid catalyzed by
266 Au@h-Al₂O₃, the reaction was carried out at different temperatures (100-

267 160 °C) in the presence of O₂ (3.0 MPa). As shown in Table S2, the yield
268 of D-xylonic acid first significantly increased from 38.6% to 83.3% when
269 reaction temperature was raised from 100 to 130 °C (Supporting
270 Information Table S2, entries 1-4), and then gradually decreased as the
271 temperature reached 160 °C (Supporting Information Table S2, entries 4-
272 7). The decreasing yield may be due to the production of byproducts (e.g.,
273 formic acid, acetic acid and lactic acid) at high temperature. The
274 selectivities of D-xylonic acid increased first and then decreased with the
275 increasing temperature (Fig. 4E), while the conversion of D-xylose
276 increased with the increase of temperature (Fig. 4F), implying
277 endothermic nature of the overall reaction. Thus, 130 °C was chosen as
278 the optimal reaction temperature. After that, the reaction was tested under
279 different O₂ pressure. It was found that only 14.7% of D-xylonic acid was
280 obtained when air was used as oxidizer (Supporting Information Table S3,
281 entry 1). As the O₂ pressure increased to 3.0 MPa, the yield remarkably
282 increased from 14.7% to 83.3% (Supporting Information Table S3,
283 entries 1-6). A slight decrease of D-xylonic acid yield (79.6%)
284 (Supporting Information Table S3, entry 7), however, was observed when
285 O₂ pressure increased to 4.0 MPa. The selectivity of D-xylonic acid under
286 different O₂ pressure also showed similar change to that of the yield of D-
287 xylonic acid, and the conversion of D-xylose increased with the increase
288 of O₂ pressure (Supporting Information Fig. 4E and 4F).



289

290 **Fig. 4** The model of D -xylose adsorption energy on Al_2O_3 (110) (A) and O_2
 291 dissociation energy on the interface of Au and Al_2O_3 in $\text{Au}@h\text{-Al}_2\text{O}_3$ (B and C)
 292 calculated by DFT (grey: C, white: H, pink: Al, red: O, yellow: Au). (D) Proposed
 293 reaction mechanism for the base-free oxidation of D -xylose to D -xylonic acid
 294 catalyzed by $\text{Au}@h\text{-Al}_2\text{O}_3$ (left) and oxygen dissociation reaction mechanism (right).
 295 The selectivity of D -xylonic acid (E) and conversion of D -xylose catalyzed (F) by
 296 $\text{Au}@h\text{-Al}_2\text{O}_3$ under different temperatures and oxygen pressures. The selectivity of D -

297 xylonic acid (G) and conversion of D -xylose (H) catalyzed by $Au@h-Al_2O_3$ under
298 different reaction times and catalyst dosages.

299 The dosage (relative to 0.25 g D -xylose) of $Au@h-Al_2O_3$ also played
300 an important role in the aerobic oxidation of D -xylose to D -xylonic acid.
301 The yield of D -xylonic acid increased with increasing dosage of $Au@h-$
302 Al_2O_3 (Supporting Information Table S4, entries 1-4). An increase in
303 dosage from 20 to 30 mg, however, did not lead to a significant increase
304 in the yield of D -xylonic acid (Supporting Information Table S4, entries
305 4-5). It is possible that D -xylose molecules adsorbed on the Al_2O_3 shell
306 became unstable species (more active), which reduced the activation
307 energy of the reaction. Similar trend was observed for the selectivity of D -
308 xylonic acid, as shown in Fig. 4G. The conversion of D -xylose increased
309 with increasing dosage of $Au@h-Al_2O_3$ (Fig. 4H). Therefore, 20 mg of
310 $Au@h-Al_2O_3$ is optimal for this reaction. Furthermore, the effect of
311 reaction time on the oxidation of D -xylose was also examined. With the
312 growth of reaction time, both the yield (Supporting Information Table S5,
313 entries 1-4) and selectivity (Fig. 4G) increased, and then decreased after
314 60 min. This phenomenon might be due to the generation of byproduct
315 (e.g., formic acid and acetic acid) from the produced D -xylonic acid with
316 increasing reaction time (Supporting Information Table S5, entries 4-6).
317 The conversion of D -xylose also increased with the increase of reaction
318 time (Fig. 4H). Furthermore, the D -xylonic acid yield and the conversion
319 of D -xylose decreased slightly from 83.3% to 80.5% and from 93.8% to
320 92.8% in the tenth recycling run, respectively. Thus, $Au@h-Al_2O_3$ is
321 highly stable and recyclable (Supporting Information Fig. S15).

322

323

324 **Table 1.** Base-free oxidation of D -xylose with structurally different Al_2O_3 -based Au
 325 catalyst.^a

Entry	Al_2O_3 -based Au catalyst	D -Xylonic acid (%)
1	Au/ Al_2O_3	21.6
2	Au@PS- <i>co</i> -P4VP@ Al_2O_3	17.2
3	Au@ <i>h</i> - Al_2O_3	83.3
4	Au-SH-(CH ₂) ₃ -Si(OCH ₃) ₃ / Al_2O_3	9.6
5	Au-SH-(CH ₂) ₃ -Si(OCH ₃) ₃ @PS- <i>co</i> -P4VP@ Al_2O_3	5.2
6	Au-SH-(CH ₂) ₃ -Si(OCH ₃) ₃ @ <i>h</i> - Al_2O_3	13.0

326 ^[a] Typical reaction conditions: D -xylose (0.25 g), O₂ (3.0 MPa), water (25 mL),
 327 Al_2O_3 -based Au catalyst (20 mg), 130 °C, 60 min.

328 To better understand our catalyst, the catalytic efficiency of Au@*h*-
 329 Al_2O_3 was compared with those catalysts that prepared in the literatures.
 330 A series of experiments were carried out at the optimal condition and the
 331 results are presented in Table S6. Although there was no significant
 332 difference in the conversion of D -xylose between Au@*h*- Al_2O_3 and other
 333 catalysts, the yield of D -xylonic acid (thus selectivity) was different. The
 334 yield of D -xylonic acid catalyzed by Au@*h*- Al_2O_3 was significantly
 335 higher than those of other catalysts (Au/SBA-15⁴⁶: 16.8%, Au@PS-*co*-
 336 P4VP: 11.4%, SiO₂-SH-Au: 1.6%, C-SH-Au: 10.8%). Furthermore, the
 337 effect of morphology of catalyst on the oxidation of D -xylose was also
 338 investigated. As shown in Table 1, the yield of D -xylonic acid catalyzed
 339 by Au/ Al_2O_3 was higher than that catalyzed by Au@PS-*co*-P4VP@ Al_2O_3 ,
 340 while Au@*h*- Al_2O_3 showed a even higher yield than Au/ Al_2O_3 ⁴⁷,
 341 implying that the Au@*h*- Al_2O_3 catalyst with special structure can
 342 effectively promote the formation of D -xylonic acid. All these results

343 suggest that the Au@*h*-Al₂O₃ has very high catalytic activity for the
344 aerobic oxidation of *D*-xylose into *D*-xylonic acid compared to other
345 catalysts. In addition, the possible reaction pathways and descriptions was
346 given in supporting informatin (Table S7, Fig. S16 and Fig. S17)

347 To determine the catalytic sites of Au@*h*-Al₂O₃, we used 3-
348 mercaptopropyltrimethoxysilane to treat the Au@*h*-Al₂O₃, and the
349 exposed Au NPs surface was covered with sulfhydryl groups. The
350 resulting Au-SH-(CH₂)₃-Si(OCH₃)₃@*h*-Al₂O₃ (Supporting Information
351 Fig. S18) was used to catalyze *D*-xylose. Only 13.0% yield of *D*-xylonic
352 acid was obtained, which well agrees with the results of Table S6 (entries
353 3 and 4). The phenomenon suggested that the catalytic sites of Au@*h*-
354 Al₂O₃ were the exposed Au NPs surface. Hence, we proposed a plausible
355 reaction mechanism of synthesis of *D*-xylonic acid from *D*-xylose
356 catalyzed by Au@*h*-Al₂O₃ (Fig. 4D). According to the early reports,⁴⁸
357 hydrogen peroxide, as a byproduct, was produced from the aerobic
358 oxidation of glucose to gluconic acid. The hydrogen peroxide acted as an
359 oxidant to oxidize glucose. In this work, our DFT calculations showed
360 that the O₂ molecule was dissociated spontaneously on the interface of
361 Au NPs and Al₂O₃ (Fig. 4B and 4C), and *D*-xylose was preferably
362 adsorbed on Al₂O₃ (Fig. 4A and Supporting Information Fig. S14). The
363 resulting negative oxygen ion can react with water to produce O₂,
364 hydrogen peroxide and hydroxyl ions (Fig. 4D, right panel). Then the
365 isomerization reaction between *D*-xylose and chain intermediate may
366 occur in the presence of hydroxyl ions. Finally, the chain intermediate
367 was oxidized by hydrogen peroxide to produce *D*-xylonic acid.

368 **Conclusions**

369 In summary, we demonstrated a highly effective chemical method for the
370 synthesis of *D*-xylonic acid from *D*-xylose, catalyzed by Au@*h*-Al₂O₃.
371 The catalytic oxidation of *D*-xylose was facile with high yields. The
372 correlation between the unique structure and catalytic activity of Au@*h*-
373 Al₂O₃ was revealed through comparative experiments. The Al₂O₃ shell
374 played a dual role in the stabilization of Au NPs and the adsorption of *D*-
375 xylose. DFT calculations revealed that the unique structure between Au
376 NPs and Al₂O₃ provided a synergism for spontaneous dissociation of O₂,
377 and hence promoted the formation of *D*-xylonic acid. At the condition of
378 130 °C, 3.0 MPa O₂ and 60 min reaction time, the *D*-xylose conversion
379 was 93.8%, and the *D*-xylonic acid yield was 83.8%. Compared with other
380 Au supported catalysts (e.g. Au/SBA-15, SiO₂-SH-Au, Au@PS-*co*-P4VP,
381 etc.), Au@*h*-Al₂O₃ showed selectivity toward the production of *D*-xylonic
382 acid. Au@*h*-Al₂O₃ was stable after 10 rounds of catalytic recycling. This
383 work provides a new facile route to selectively oxidize monosaccharides
384 into value-added sugar acids such as *D*-xylonic acid, using a type of
385 hermit crab typological nanocatalyst Au@*h*-Al₂O₃.

386 **Experimental**

387 **Synthesis of Au@*h*-Al₂O₃ nanocatalyst**

388 The styrene was pretreated before use. First, a certain amount of
389 commercially available styrene was added into 10% sodium hydroxide
390 solution, and the system was placed stably for 10 min at 4 °C. The
391 process was replicated for 3 times. Thereafter, the styrene was washed
392 with water and dried with anhydrous magnesium sulfate overnight.
393 Finally, the pure styrene was obtained by vacuum distillation and kept at
394 4 °C.

395 The polystyrene-*co*-poly(4-vinylpyridine) (PS-*co*-P4VP) core-shell
396 microspheres were synthesized by one-stage, soap-free emulsion
397 polymerization.⁴⁹ Typically, 80 mmol of 4-vinylpyridine was mixed with
398 360 mL of water at room temperature, then 160 mmol of styrene was
399 added to the above system under magnetic stirring. The mixture was
400 stirred vigorously for another 30 min at room temperature. Thereafter,
401 1.30 g of K₂S₂O₈ was added into the reaction system, and the pH of the
402 mixture was adjusted to 7 with 0.1 mol/L HCl aqueous solution. The
403 reaction system was then filled with nitrogen and carried out at 80 °C for
404 24 h under vigorous stirring conditions. Finally, the excessive volume of
405 0.1 mol/L NaOH aqueous solution was injected into the above colloidal
406 dispersion, and the obtained precipitates were washed with deionized
407 water and then dried in a vacuum at 50 °C overnight.

408 0.480 g PS-*co*-P4VP was dispersed in HAuCl₄ aqueous solution and
409 stirred at room temperature for 17 h. After that, the pH of the mixture was
410 adjusted to 7 with 0.1 mol/L NaOH aqueous solution, and then a 5-fold
411 excess volume of 0.1 mol/L NaBH₄ aqueous solution was added drop
412 wise with vigorous stirring. The obtained Au@PS-*co*-P4VP core-shell
413 microspheres were collected by centrifugation, washed thrice with
414 deionized water, and dried in a vacuum at 80 °C.

415 A certain volume of formic acid-ammonium formate buffer solution
416 (pH = 4.4) was first prepared. Then, a certain amount of Au@PS-*co*-
417 P4VP core-shell microspheres and aluminum sulfate were added and
418 dispersed by ultrasound for 15 min. The system was carried out at 70 °C
419 for 2 h with vigorous stirring. The obtained Au@PS-*co*-P4VP@Al₂O₃
420 was collected by centrifugation, washed with deionized water and oven-
421 dried at 80 °C overnight. The Au@*h*-Al₂O₃ was obtained by calcinating

422 Au@PS-co-P4VP@Al₂O₃ at 550 °C for 4 h. Changing the concentration
423 of aluminum salts can easily tune the thickness of aluminum oxide shell.

424 **Activity Tests.** The catalytic synthesis of D-xylonic acid were
425 carried out in a 60 mL Teflon-lined stainless-steel autoclave. In a typical
426 procedure, 0.25 g D-xylose was dissolved in 25 mL water, and then a
427 certain amount of Au@h-Al₂O₃ was added into the solution and dispersed
428 by ultrasound for 10 min. Then oxygen was purged into the reactor for
429 three times before the reactor being sealed and pressurized with oxygen.
430 The reaction was then heated to a required temperature for different times
431 under constant stirring (1000 rpm). After the completion of the reaction,
432 the autoclave was immersed in a water bath to cool down, and the oxygen
433 was expelled from the stainless-steel autoclave at the same time. Finally,
434 the sample was immediately syringed out, filtered and analyzed by high-
435 performance liquid chromatography (HPLC, Agilent 1260 series) with a
436 UV detector.

437 **Conflicts of interest**

438 The authors declare no conflict of interest.

439 **Acknowledgements**

440 We wish to thank for the Natural Science Foundation of China (31430092,
441 21506068, 21736003, 21576094), Guangdong Natural Science Funds for
442 Distinguished Young Scholar (2016A030306027, 2017A030306029),
443 Tip-top Scientific and Technical Innovative Youth Talents of Guangdong
444 Special Support Program (2015TQ01C488), Guangdong Natural Science
445 Foundation (2017A030313130), State Key Laboratory of Pulp and Paper
446 Engineering and Fundamental Research Funds for the Central

447 Universities. We also thank to the Qian Liu from shiyanjia lab
448 (www.shiyanjia.com) for the XPS analysis.

449 **Notes and references**

450 1 Z. L. Zhang and G. W. Huber, *Chem. Soc. Rev.*, 2018, **47**, 1351-1390.

451 2 V. G. Goz, I. Pinter, V. Harmat and A. Perczel, *Eur. J. Org. Chem.*,
452 2018, **3**, 355-361.

453 3 J. J. Liu, J. H. Li, H. D. Shin, L. Liu, G. C. Du, and J. Chen,
454 *Bioresource Technol.*, 2017, **239**, 412-421.

455 4 S. P. N. Ayudthaya, A. H. P. van de Weijer, A. H. van Gelder, A. J. M.
456 Stams, W. M. de Vos and C. M. Plugge, *Biotechnol. Biofuels*, 2018, **11**,
457 1-15.

458 5 M. Toivari, M. L. Vehkomaki, Y. Nygard, M. Penttila, L. Ruohonen
459 and M. G. Wiebe, *Bioresource Technol.*, 2013, **133**, 555-562.

460 6 J. H. Van Vleet and T. W. Jeffries, *Curr. Opin. Biotechnol.*, 2009, **20**,
461 300-306.

462 7 S. J. Kim, H. J. Sim, J. W. Kim, Y. G. Lee, Y. C. Park and J. H. Seo,
463 *Bioresource Technol.*, 2017, **245**, 1551-1557.

464 8 H. X. Fu, L. Yu, M. Lin, J. F. Wang, Z. L. Xiu and S. T. Yang, *Metab.*
465 *Eng.*, 2017, **40**, 50-58.

466 9 H. Liu, K. N. G. Valdehuesa, G. M. Nisola, K. R. M. Ramos and W. J.
467 Chung, *Bioresource Technol.*, 2012, **115**, 244-248.

468 10 J. S. Martin del Campo, J. Rollin, S. Myung, Y. Chun, S. Chandrayan,
469 R. Patino, M. W. W. Adams and Y. H. P. Zhang, *Angew. Chem. Int.*
470 *Edit.*, 2013, **52**, 4587-4590.

- 471 11 W. Niu, M. N. Molefe and J. W. Frost, *J. Am. Chem. Soc.*, 2003, **125**,
472 12998-12999.
- 473 12 B. W. Chun, B. Dair, P. J. Macuch, D. Wiebe, C. Porteneuve and A.
474 Jeknavorian, *Appl. Biochem. Biotech.*, 2006, **129**, 645-658.
- 475 13 J. L. Ma, L. X. Zhong, X. W. Peng and R. C. Sun, *Green Chem.*, 2016,
476 **18**, 1738-1750.
- 477 14 Y. Tomoda, A. Hanaoka, T. Yasuda, T. Takayama, A. Hiwatashi, Y.
478 Tomota, T. Hanaoka, S. Takayama and A. Hiwatari, *US Patent*, 2004,
479 2004131737-A1.
- 480 15 P. Pujos, M. H. Jijakli, P. Philippe, M. H. Jujakli and M. Haissam
481 Jujakli, *Patent*, 2006, WO2006032530-A1.
- 482 16 L. B. Lockwood, G. E. Nelson, *J. Bacteriol.*, 1946, **52**, 581-596.
- 483 17 Y. Nygard, M. H. Toivari, M. Penttila, L. Ruohonen, M. G. Wiebe,
484 *Metab. Eng.*, 2011, **13**, 383-391.
- 485 18 M. H. Toivari, L. Ruohonen, P. Richard, M. Penttila, M. G. Wiebe,
486 *Appl. Microbiol. Biot.*, 2010, **88**, 751-760.
- 487 19 A. S. Dahms, *Biochem. Biophys. Res. Commun.*, 1974, **60**, 1433-1439.
- 488 20 N. Tenhaef, C. Brusseler, A. Radek, R. Hilmes, P. Unrean, J.
489 Marienhagen, S. Noack, *Bioresour. Technol.*, 2018, **268**, 332-339.
- 490 21 S. Biella, L. Prati and M. Rossi, *J. Catal.*, 2002, **206**, 242-247.
- 491 22 H. Sakamoto, J. Imai, Y. Shiraishi, S. Tanaka, S. Ichikawa and T.
492 Hirai, *ACS Catal.*, 2017, **7**, 5194-5201.
- 493 23 S. J. Kim, S. J. Choi, J. S. Jang, H. J. Cho, W. T. Koo, H. L. Tuller
494 and I. D. Kim, *Adv. Mater.*, 2017, **29**, 1-9.

- 495 24 J. F. Yu, Q. Wang, D. O'Hare and L. Y. Sun, *Chem. Soc. Rev.*, 2017,
496 46, 5950-5974.
- 497 25 D. M. Meng, Q. Xu, Y. L. Jiao, Y. Guo, Y. L. Guo, L. Wang, G. Z. Lu
498 and W. C. Zhan, *Appl. Catal. B-environ.*, 2018, **221**, 652-663.
- 499 26 M. Baya, U. Belio, I. Fernandez, S. Fuertes and A. Martin, *Angew.*
500 *Chem. Int. Edit.*, 2016, **55**, 6978-6982.
- 501 27 J. Su, C. L. Xie, C. Chen, Y. Yu, G. Kennedy, G. A. Somorjai and P.
502 D. Yang, *J. Am. Chem. Soc.*, 2016, **138**, 11568-11574.
- 503 28 J. B. Song, F. Wang, X. Y. Yang, B. Ning, M. G. Harp, S. H. Culp, S.
504 Hu, P. Huang, L. M. Nie, J. Y. Chen and X. Y. Chen, *J. Am. Chem.*
505 *Soc.*, 2016, **138**, 7005-7015.
- 506 29 M. T. Zhao, K. Yuan, Y. Wang, G. D. Li, J. Guo, L. Gu, W. P. Hu, H.
507 J. Zhao and Z. Y. Tang, *Nature*, 2016, **539**, 76-80.
- 508 30 M. A. Khalily, H. Eren, S. Akbayrak, H. H. Susapto, N. Biyikli, S.
509 Ozkar and M. O. Guler, *Angew. Chem. Int. Edit.*, 2016, **55**, 12257-
510 12261.
- 511 31 X. Q. Liu, J. Iocozzia, Y. Wang, X. Cui, Y. H. Chen, S. Q. Zhao, Z. Li
512 and Z. Q. Lin, *Energy Environ. Sci.*, 2017, **10**, 402-434.
- 513 32 B. Cai, R. Hubner, K. Sasaki, Y. Z. Zhang, D. Su, C. Ziegler, M. B.
514 Vukmirovic, B. Rellinghaus, R. R. Adzic and A. *Angew. Chem. Int.*
515 *Edit.*, 2018, **57**, 2963-2966.
- 516 33 S. Wu, J. Dzubiella, J. Kaiser, M. Drechsler, X. H. Guo, M. Ballauff
517 and Y. Lu, *Angew. Chem. Int. Edit.*, 2012, **51**, 2229-2232.

- 518 34 L. S. Lin, X. Y. Yang, Z. J. Zhou, Z. Yang, O. Jacobson, Y. J. Liu, A.
519 Yang, G. Niu, J. B. Song, H. H. Yang and X. Y. Chen, *Adv. Mater.*,
520 2017, **29**, 1-9.
- 521 35 J. J. Wei, K. Niikura, T. Higuchi, T. Kimura, H. Mitomo, H. Jinnai, Y.
522 Joti, Y. Bessho, Y. Nishino, Y. Matsuo and K. Ijio, *J. Am. Chem. Soc.*,
523 2016, **138**, 3274-3277.
- 524 36 C. Wu, P. Kopold, P. A. van Aken, J. Maier and Y. Yu, *Adv. Mater.*,
525 2017, **29**, 1-7.
- 526 37 G. D. Park, J. K. Lee and Y. C. Kang, *Adv. Funct. Mater.*, 2017, **7**, 1-9.
- 527 38 M. B. Gawande, A. Goswami, T. Asefa, H. Z. Guo, A. V. Biradar, D.
528 L. Peng, R. Zboril and R. S. Varma, *Chem. Soc. Rev.*, 2015, **44**, 7540-
529 7590.
- 530 39 R. J. Ren, L. Q. Xu, L. Zhu, X. Y. Wang, X. J. Ma, D. B. Wang, *ACS*
531 *Appl. Mater. Inter.*, 2018, **10**, 11642-11651.
- 532 40 J. W. Feng, J. Liu, X. Y. Cheng, J. J. Liu, M. Xu, J. T. Zhang, *Adv.*
533 *Sci.*, 2018, **5**, 1-7.
- 534 41 F. Wen, W. Q. Zhang, G. W. Wei, Y. Wang, J. Z. Zhang, M. C. Zhang
535 and L. Q. Shi, *Chem. Mater.*, 2008, **20**, 2144-2150.
- 536 42 W. Zhang, X. J. Lin, Y. G. Sun, D. S. Bin, A. M. Cao and L. J. Wan,
537 *Appl. Mater. Interfaces*, 2015, **7**, 27031-27034.
- 538 43 J. Zhang, Y. Jin, C. Y. Li, Y. N. Shen, L. Han, Z. X. Hu, X. W. Di and
539 Z. L. Liu, *Appl. Catal. B-environ.*, 2009, **91**, 11-20.
- 540 44 Dassault Systèmes BIOVIA, Materials Studio 2017, San Diego:
541 Dassault Systèmes, 2017.

542 45 N. Sharifi, C. Falamaki and M. G. Ahangari, *Appl. Surf. Sci.*, 2017,
543 **416**, 390-396.

544 46 A. Kumar, V. P. Kumar, A. Srikanth, V. Vishwanathan and K. V. R.
545 Chary, *Catal. Lett.*, 2016, **146**, 35.

546 47 A. V. Chistyakov, P. A. Zharova, S. A. Nikolaev and M. V. Tsodikov,
547 *Catal. Today*, 2017, **279**, 124.

548 48 M. Comotti, C. Della Pina, E. Falletta and M. Rossi, *Adv. Synth.*
549 *Catal.*, 2006, **348**, 313-316.

550 49 F. Wen, W. Q. Zhang, G. W. Wei, Y. Wang, J. Z. Zhang, M. C. Zhang
551 and L. Q. Shi, *Chem. Mater.* 2008, **20**, 2144-2150.

552

553